ANALYSIS OF FIVE-POINT BENDING TEST FOR MULTILAYER SURFACING SYSTEM ON ORTHOTROPIC STEEL BRIDGE

J. Li[1], X.Liu[2], A. Scarpas[3], G. Tzimiris[4], C. Kasbergen[5], R. Hofman[6], J. Voskuilen[7]

[1] Corresponding author
Section of Structural Mechanics, Delft University of Technology
Stevinweg 1, 2628 CN Delft, the Netherlands
Phone: + 31 (0)15 27 84676
Email: jinlong.li@tudelft.nl

[2] Section of Structural Mechanics, Delft University of Technology
Stevinweg 1, 2628 CN Delft, the Netherlands
Phone: + 31 (0)15 27 87918
Email: x.liu@tudelft.nl

[3] Section of Structural Mechanics, Delft University of Technology
Stevinweg 1, 2628 CN Delft, the Netherlands
Phone: + 31 (0)15 27 84017
Email: a.scarpas@tudelft.nl

[4] Section of Structural Mechanics, Delft University of Technology
Stevinweg 1, 2628 CN Delft, the Netherlands
Phone: + 31 (0)15 27 89388
Email: g.tzimiris@tudelft.nl

[5] Section of Structural Mechanics, Delft University of Technology
Stevinweg 1, 2628 CN Delft, the Netherlands
Phone: + 31 (0)15 27 82729
Email: c.kasbergen@tudelft.nl

[6] Rijkswaterstaat, Centre for Traffic and Navigation
Schoenmakerstraat, 2628 VK Delft, the Netherlands
Phone: + 31 (0)887982284
Email: rob.hofman@rws.nl

[7] Rijkswaterstaat, Centre for Traffic and Navigation
Schoenmakerstraat, 2628 VK Delft, the Netherlands
Phone: + 31 (0)88 7982304
Email: jan.voskuilen@rws.nl

Submission Date: 19/07/2012

Word Count:

Body Text   = 3052

Abstract   = 190

Figures 16×250 = 4000

Tables 1×250 = 250

Total   = 7492

ABSTRACT

The French five-point bending test (5PBT) provides a laboratory scale test that allows studying the fatigue resistance of surfacing systems on orthotropic steel deck bridges (OSDB). The surfacing structure for OSDB in the Netherlands consists mostly of multilayer system: top porous asphalt layer, guss asphalt layer, steel deck and two membrane layers. In this paper, an analytical solution for 5PBT setup is presented first. In order to better understand the influence of geometrical, mechanical and structural parameters on the performance of the typical multilayer surfacing system of OSDB in the Netherlands, the 5PBT specimens with five structural layers have been investigated. The parametric study is performed at the numerical platform CAPA-3D that was developed at the Section of Structural Mechanics of TU Delft. The thicknesses of the top porous asphalt layer, middle guss asphalt layer and the steel plate are varied. The influences of the mechanical properties of both top and bottom membrane layers are studied. The sensitivities of those influence factors are evaluated by the examination of the maximum tensile stress at the top surface of the porous asphalt layers and the strain distributions through the entire thickness of the specimen at two cross sections.

Keywords: five-point bending test; orthotropic steel deck bridge; surfacings; membrane; finite
            element analysis

1   **INTRODUCTION**

2   Orthotropic steel bridges are widely used in most of the major long span bridges around the world.
3   The lightweight and flexibility make OSDB a prior cost-effective solution for cases where a high
4   degree of pre-fabrication or rapid erection is required *(1)*, in seismic zones, for movable bridges, long-
5   span bridges and for rehabilitation to reduce bridge weight *(2)*.
6   An OSDB consists of a deck plate supported in two mutually perpendicular directions by a
7   system of longitudinal stiffeners and transverse crossbeams. Usually the deck plate is surfaced by
8   bituminous wearing courses. It is known that surfacings reduce the stresses in the steel structure
9   except for their functions of skid resistance or waterproofing. In the Netherlands an asphaltic
10 surfacing structure for OSDB mostly consists of two structural layers. The upper layer consists of
11 porous asphalt (PA) because of reasons related to noise hindrance. For the lower layer a choice
12 between mastic asphalt (MA), or guss asphalt (GA), can be made *(3)*. There are two layers of
13 membrane layers are needed to bond the two structure layers together. Earlier investigations have
14 shown that the bonding strength of membrane layers to the surrounding materials has a strong
15 influence on the structural response of OSDB. The most important requirement for the application of
16 membrane materials is that the membrane adhesive layer shall be able to provide sufficient bond to
17 the surrounding materials.
18   In the last three decades, several problems were reported in relation to asphaltic surfacing
19 materials on OSDB such as rutting, cracking, loss of bond between the surfacing material and the
20 steel plate. Better understanding of the response of the multilayer surfacings as well as fine modeling
21 of their behavior are required in order to improve the current design method so as to prolong the
22 service life of the surfacings on OSDB.
23   The five-point bending test (5PBT) was developed in France by the Laboratoire Central des
24 Ponts et Chaussées (LCPC) in the 1970's *(4)*. This is a capable test that is essential for the design of
25 the asphalt layers on bridge decks because of its reliable testing results are consistent with in situ
26 observations on real steel decks.
27   In this paper, finite element (FE) simulations of 5PBT with two membrane layers surfacing
28 system are presented. The finite element system CAPA-3D *(5)* developed at the Section of Structural
29 Mechanics of TU Delft has been utilized as the numerical platform for this study. The goal of this
30 study is to develop efficient numerical and analytical techniques for optimization of the multilayer
31 system composed of asphaltic mixes, top and bottom membranes as well as the interfaces with proper
32 mechanical properties. The influences of two asphaltic surfacing materials, two membranes and four
33 interface layers are quantified systematically. The non-linear material models and the material
34 properties are derived and utilized to characterize the mechanical behavior of the asphaltic surfacing
35 materials. In the end to come up with a guidance for engineers who are involved with deck-pavement
36 designs.
37

COMPARABILITY BETWEEN 5PBT AND ORTHOTROPIC STEEL BRIDGE

When a dual wheel load is applied onto an steel deck surfacing, a typical deformation could be obtained as shown in Figure 1 left. Transversal tensile deformations are observed at upper locations in middle of the dual wheel load as well as the lower parts of those surfacing layers under the wheel load. The three stiffeners could be regarded as exactly the three supporters in 5PBT.


Five-point bending test
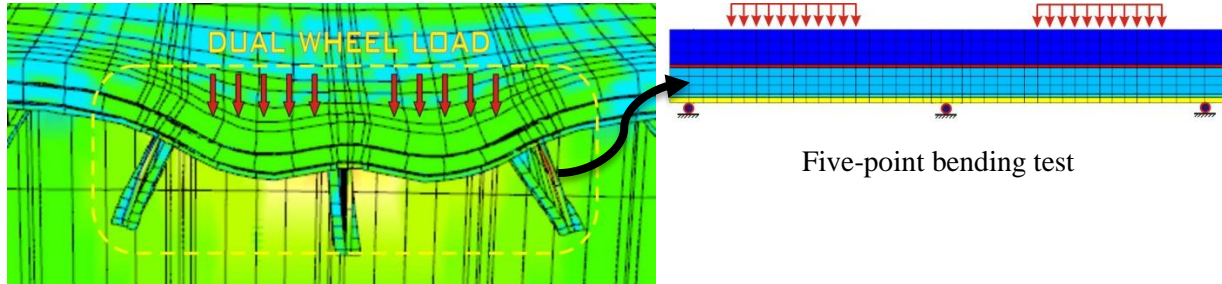
FIGURE 1 Schematic show of a dual wheel load on OSDB and 5PBT

The 5PBT is a laboratory scale test that allows studying the fatigue resistance of surfacing layers on OSDB. Hameau et al. (1981) report the most severe load case for surfacing layers of OSDB is when they are subjected to negative moments. During the 5PBT tests, high stress concentration at the location in the middle of the test specimen is produced. The 5PBT has become a French standard test method (NF-P98-286, 2006) and has been used in several studies *(6)(7)(8)*.

ANALYTICAL SOLUTION OF 5PBT

In this section, the deduction of analytical solution for 5PBT setup is presented. The mechanical model used for carrying out the analytical study is a two-span continuous beam, Figure 2 (a).

(a)   (b)
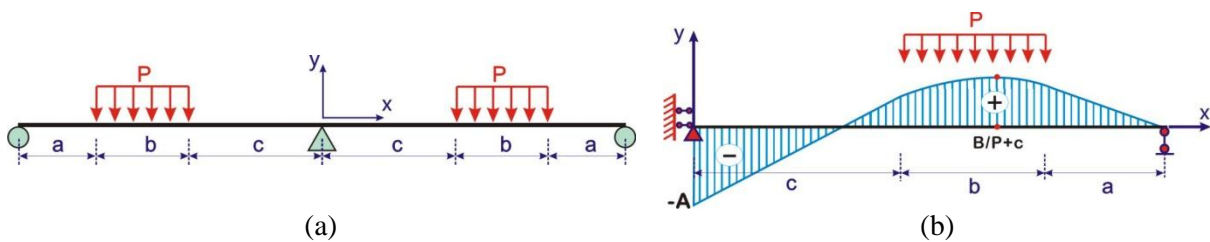
FIGURE 2 (a) Beam model of 5PBT for analytical study; (b) Half of the model due to symmetry

Figure 2(a) shows the beam-model where x, y are the axes in the direction of the length and thickness respectively. The two-span beam is symmetric by the middle support, with each span length $a+b+c$. The two distribution loads have a length of b. The loading area has a distance a from the beam end and a distance c to the middle support. Because of symmetry, half of the two-span continuous beam is plotted in Figure 2(b).

This is a statically indeterminate structure. By using force method, the moment distribution function along the beam can be expressed by:

$$M = \begin{cases} -A + Bx & 0 \le x < c \\ -A + Bx - \dfrac{P(x-c)^2}{2} & c \le x < b+c \\ C\left(1 - \dfrac{x}{a+b+c}\right) & b+c \le x < a+b+c \end{cases} \qquad (1)$$

in which:

$$A = \frac{Pb(4ba^2 + 8ca^2 + 12abc + 4b^2a + 4c^2a + 2bc^2 + b^3 + 4b^2c)}{8(a+b+c)^2};$$

62
$$B = \frac{Pb(24ba^2 + 24ca^2 + 36abc + 20b^2a + 12c^2a + 6bc^2 + 5b^3 + 12b^2c + 8a^3)}{8(a+b+c)^3};$$

63
$$C = \frac{Pb(12abc + 4ab^2 + 12ac^2 + 18bc^2 + 3b^3 + 12b^2c + 8c^3)}{8(a+b+c)^2}.$$

64   The maximum negative bending moment is located at the center support (x=0); The maximum
65   positive bending moment is located at $x = B/P + c$ .The analytical bending moment distribution is
66   shown in Figure 3. The longitudinal strain (strain x) distribution can be easily computed on the basis
67   of the moment function and section properties of the specimen.

68   For the 5PBT setup we used in the test, a=45mm, b=130mm and c=95mm, and distribution
69   load P=0.707MPa was applied. In order to verify the analytical solution of Equation (1), a 5PBT test
70   on a steel specimen has been done. Three strain gauges were placed to record the strains in the middle
71   of the specimen and under the two loading foots respectively. Besides, FE simulation for this 5PBT
72   on the steel specimen with elastic modulus E=210GPa and Poisson's ratio 0.2 was also done by
73   CAPA-3D. The transversal strains along x axis direction obtained from those three methods show the
74   great agreement, see Figure 3.
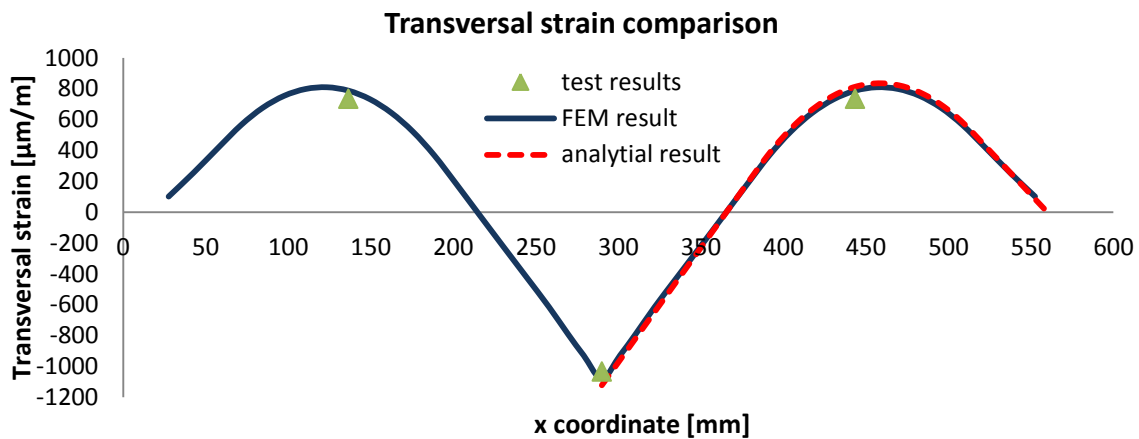
75

76   **FIGURE 3 Verification of analytical solution of 5PBT**

77   **FINITE ELEMENT SIMULATIONS OF 5PBT**

78   Finite element simulations were performed by CAPA3D FE package that was developed at the
79   Section of Structural Mechanics of TU Delft.
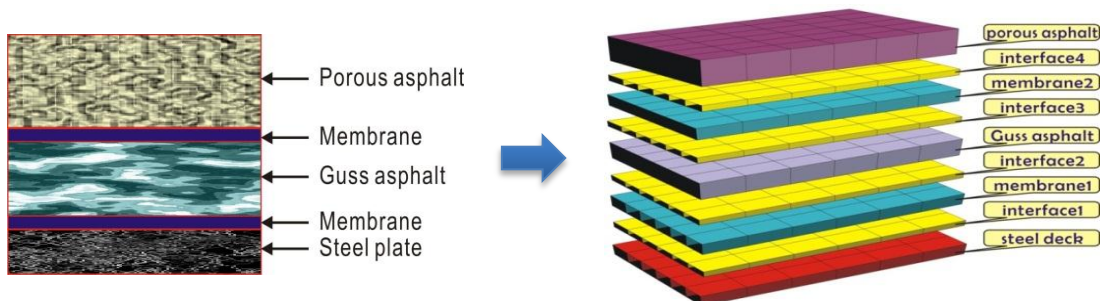
80   **FIGURE 4 Schematic diagram of the FE surfacing layers**
81   Three-dimensional finite elements are used in building the model of 5PBT. The porous
82   asphalt(PA) layer, guss asphalt(GA) layer, top membrane(TM) layer, bottom membrane(BM) layer
83   and the steel deck plate were modelled by using 20-nodes brick (solid) elements, Figure 4. A new
84   contact interface element based on the previous work by X. Liu and A. Scarpas *(9)* was used to

85 describe the four interface layers between those surfacing layers. A cohesive traction-separation law is
86 utilized in the contact element.

Geometry and boundary conditions of 5PBT mesh

88 The geometry of 5PBT is shown in Figure 5. The specimen is 580 mm in length and 100 mm in width.
89 The thicknesses of PA, GA, TM, BM and the steel deck are adjustable to test their effects on the
90 mechanical response of the specimen. Two side supports locate at the distance 270 mm from the
91 central support. Total 1677 elements is utilized for the simulation. Two loading shoes with each
92 dimensions 130×100 mm locate 65 mm from the ends of the specimen. The pressure load applied on
93 each shoe was 0.707MPa. This load pressure corresponds with 9.2 kN on each shoe (0.707MPa x
94 130mm x 100mm), which means a total of 18.4kN. If the same pressure load of 0.707MPa is applied
95 on a wheel print type B (double tyre 220mm by 320mm), it corresponds with 100kN wheel load
96 which is typical truck load utilized in the Netherland.
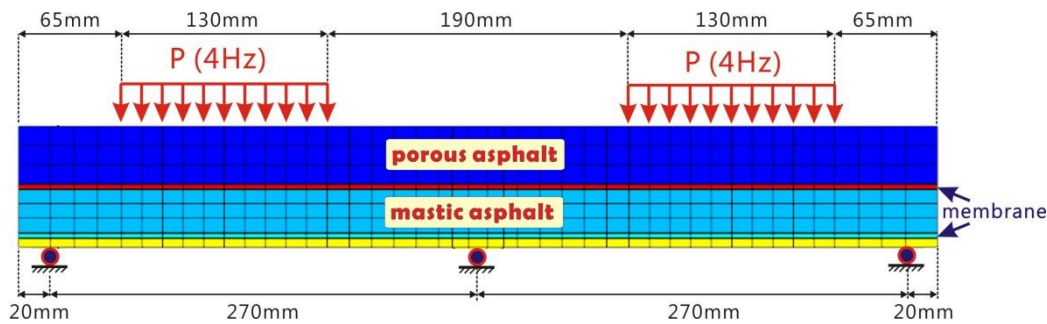
97

98   **FIGURE 5 Geometry and boundary conditions of 5PBT FE model**

Material models and parameters of the surfacing materials

100 *Asphaltic materials*

101 As shown in Figure 4, in the Netherlands, the surfacing structure for OSDB mostly consists of two
102 structural layers. The upper layer consists of porous asphalt (PA) and the lower layer consists a choice
103 between mastic asphalt (MA), or guss asphalt (GA). Two layers of membrane layers are needed to
104 bond the two structure layers together.
105 the membranes products are mostly made by bitumen-based materials, thereby the mechanical
106 responses of the asphalt surfacing layers and the membrane material are time dependent and
107 temperature sensitive. In order to simulate the surfacing layer response properly, a Visco-Elastic
108 Zener model is utilized for the finite element studies.
109   The reason of choosing the Visco-Elastic Zener model for this finite element is because its
110 constitutive relation is simple and the model parameter can be easily determined by the conventional
111 experimental tests, i.e. creep test or relaxation test. Figure 6 shows the mechanical analog of this
112 viscoelastic Zener model.
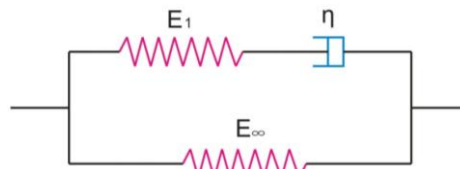
113
114   **FIGURE 6 Schematic diagram of Zener model**
115   The model consists of two parallel components. One is purely elastic with modulus E_∞ and the
116 other is viscoelastic consisting of a spring with modulus E_1 and a damper with viscosity coefficient η
117 in series.

118   The total stress σ can be decomposed in two components, one is the stress σ_1 in the
119   viscoelastic component and the other is the stress σ_2 in the elastic component. It can be expressed as
120   follow

$$\sigma = \sigma_1 + \sigma_2 = E_\infty \varepsilon + E_1 \left(\varepsilon - \varepsilon_v \right)$$
$$E_1 \left(\varepsilon - \varepsilon_v \right) = \eta\, \dot{\varepsilon}_v$$

(2)

121

122   in which $\varepsilon_v = \varepsilon(t) - \varepsilon(0)\exp\left(-\dfrac{E_1}{\eta}t\right) - \int\limits_0^t \exp\left(-\dfrac{E_1}{\eta}(t-\tau)\right)\dot{\varepsilon}(\tau)d\tau$ is the viscous strain of

123   the material and $\varepsilon(0)$ is the initial strain at time zero.

124   *Interface layers*

125   A contact interface element based on the previous work by X. Liu and A. Scarpas *(9)* within the FE
126   package CAPA-3D is utilized to model the cohesive behavior of the membranes and the surrounding
127   surfacing materials causing into contact.
128   The contact interface element developed is based on the classical 16-noded interface element.
129   It consists of two opposite faces each with 8 nodes. The thickness of the element in its un-deformed
130   configuration can be specified to any initial value.
131   A cohesive traction-separation law is utilized to prevent the contact interface to freely
132   separate as soon as it undergoes tensile forces, see Figure 7(a).
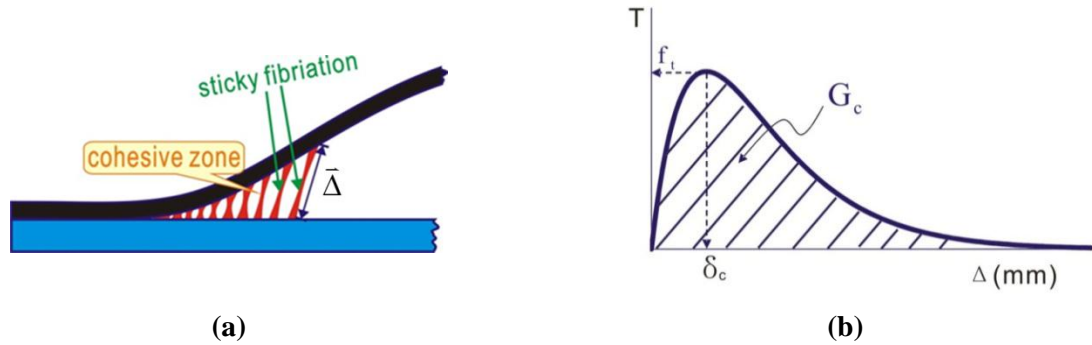

(a)   **(b)**
**FIGURE 7(a) Schematic of traction separation at contact interface; (b) Schematic traction-
separation relation**

133   Interfacial fibrillation is a typical mechanism that frequently occurs during debonding of
134   membranes from substrates, see Figure 7(a). It involves large displacements at the interface as well as
135   large deformations in the membrane material. Therefore, a generic cohesive zone model is introduced
136   that is suitable to describe the process of membrane debonding from substrate.
137   The cohesive zone law which is utilized to describe the traction-separation relation of
138   fibrillation is controlled by one constitutive relation between traction force and the opening
139   displacement along the fibril axis, Figure 7(a). Under large displacements, it is no longer physical to
140   discriminate between normal and tangential openings, in the case of membrane debonding from
141   substrates, such large displacements are bridged by fibrils, which at more or less like non-liner springs
142   can only transfer a load along their axis.
143   The cohesive law proposed here *(10)* is defined as:

$$T = \frac{G_c}{\delta_c}\left(\frac{\Delta}{\delta_c}\right)\exp\left(-\frac{\Delta}{\delta_c}\right)$$

(3)

144

145   where G_c is the strain energy release rate which is characterized as the energy per unit crack length
146   required for crack/debonding extension. δ_c is a characteristic opening length. The maximum traction
147   f_t is related to G_c and δ_c, see Figure 7(b).

148   **NUMERICAL PARAMETRIC STUDY**

149   Finite element (FE) analysis is performed to better understand the composite behavior of the
150   multilayer surfacing system. The coordinate axis x, y and z are in the direction of the length, thickness
151   and width of the specimen. Five cases are simulated and analyzed in order to identify the sensibilities
152   of those factors:
153   • Thickness and stiffness of porous asphalt layer;
154   • Thickness and stiffness of guss asphalt layer;
155   • Stiffness of upper and bottom membrane layers;
156   • Thickness of steel deck plate,
157   • Environmental temperatures of $10\,^{\circ}$C and $-5\,^{\circ}$C.
158   The transversal strain distribution at two cross sections of the structure are outputted and
159   compared. The two studied sections are shown in Figure 8 below.
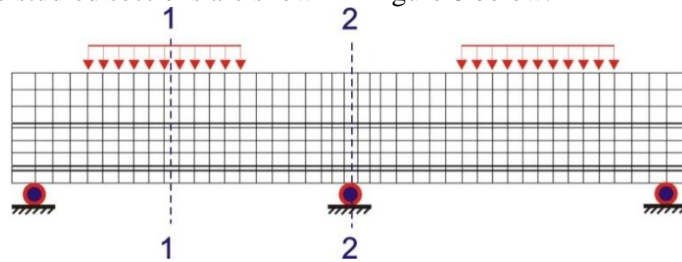
160
161   **FIGURE 8 Two cross sections of the FE mesh where strain & stress are outputted**
162   In this study, the four fully bonded interface layers are utilized, thus not debond occurs in our
163   finite element simulations. Steel is regarded as a linear elastic material with Young's modulus 210000
164   MPa and the Poisson's ratio 0.2. Asphalt surfacing materials are assumed to be viscoelastic. Model
165   parameters at 10 and -5 degrees were determined by relaxation tests and were validated by five-point
166   bending tests (Table 1). Details of determination of those parameters are beyond the scope of this
167   paper.

168   **TABLE 1 Parameters of VE materials**

temperature($^{\circ}$C)	material layer	E_1(MPa)	E_∞ (MPa)	Poisson's ratio	η (MPa.s)
	Porous asphalt	200	1	0.3	15750
10	Guss asphalt	450	3	0.3	15750
	Upper/bottom membrane	9.18	5.9	0.3	267
	Porous asphalt	2000	10	0.3	22500
-5	Guss asphalt	4500	30	0.3	22500
	Upper/bottom membrane	46	30	0.3	384

169

170

Effect of the thicknesses of porous asphalt

171

172   A group of simulations are done by varying the thickness of PA layer from 30 mm to 70 mm. The
173   longitudinal strain (strain xx) at sections 1-1 and 2-2 (Figure 8) are shown in Figure 9.
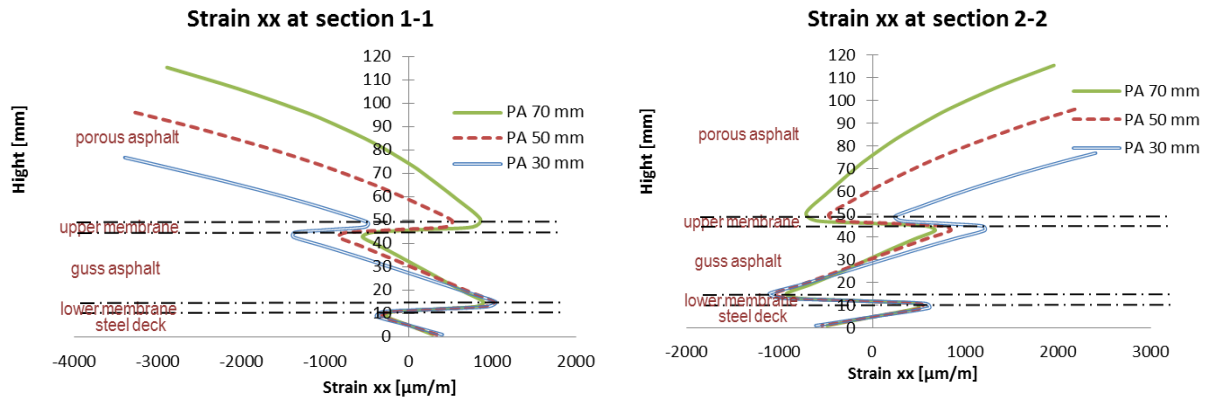

FIGURE 9 Transversal strain at section 1-1 & 2-2 (PA thickness varies)

174   The following observations are made with respect to the results shown in Figure 9.

175   •   The distribution of the longitudinal strain ε_{xx} follows more or less the same pattern in the
176   5PBT with three different thicknesses of PA. By varying the thickness of the PA layer, the
177   strain distributions both in PA and GA are effected. However less effects can be observed in
178   the steel deck plate by this variance.
179   •   Maximum tensile strains in the two structural layers (PA & GA) are reduced by an increasing
180   thickness of PA.
181   Figure 10 shows the maximum tensile strain above the middle support on the top of PA
182   versus the PA thickness variation. It can be observed that a 10 mm thicker porous asphalt layer may
183   reduce the maximum tensile strain on top of PA layer by 5%. This maximum tensile strains always
184   capture the attention of engineers since most of the cracks occurs in OSDB are relevant with those.
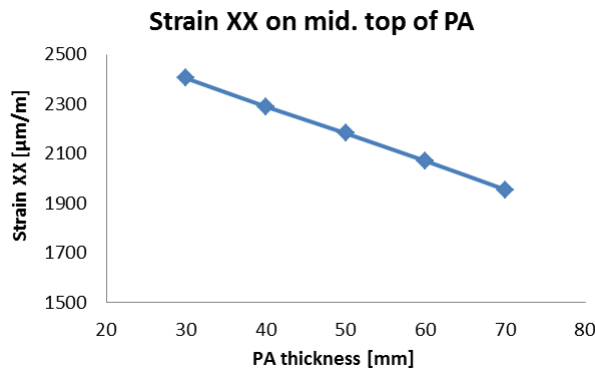

**FIGURE 10 Maximum transversal tensile strain on top of PA (PA thickness
varies)**

Effect of the thickness of guss asphalt layer

185

186   Similar simulations are done by varying the thickness of GA layer from 20 mm to 60 mm. The
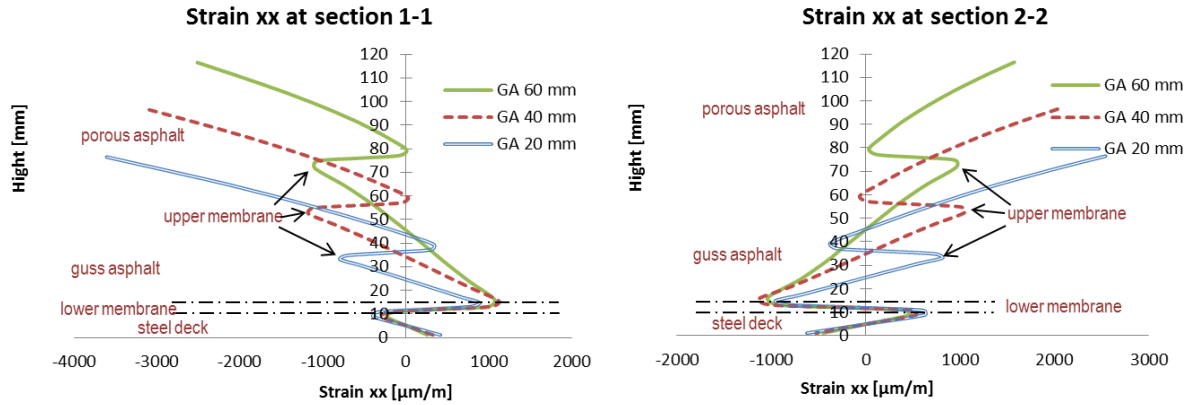187   longitudinal strain (strain xx) at the two studied sections (Figure 8) are shown in Figure 11.

FIGURE 11 Longitudinal strain at section 1-1 & 2-2 (GA thickness varies)

188 From Figure 11 the following remarks can be made:

189 • The distribution of the longitudinal strain ε_{xx} follows more or less the same pattern in the
190 5PBT simulations with three different thicknesses of GA. Similar as the previous PA case, by
191 varying the thickness of the GA layer, the strain distributions both in PA and GA are effected.
192 However less effects can be observed in the steel deck plate by this variance.
193 • Both maximum tensile and compressive strains in GA layer are more or less the same. While
194 the maximum tensile strain in PA layer is reduced significantly by increasing the GA
195 thickness.
196 Figure 12 shows the maximum tensile strain above the middle support on the top of PA
197 versus the GA thickness variation. It is observed that a 10 mm thicker GA layer may reduce
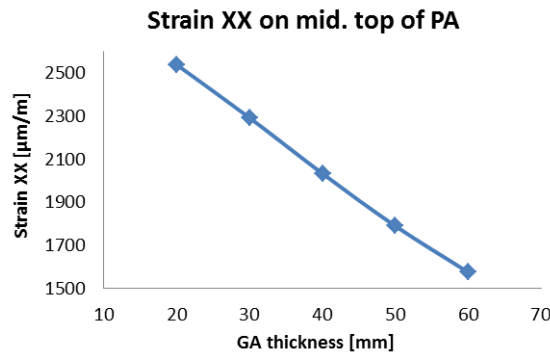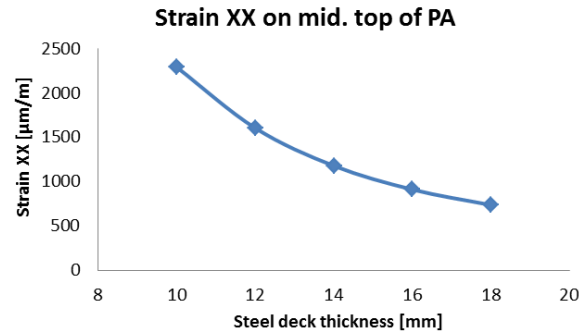198 the maximum tensile strain on top of PA layer by 11%.

199

200

201 **FIGURE 12 Maximum tensile strain on top of PA (GA thickness varies)**

202 **Effect of the thickness of steel deck**

203 Five cases with steel deck thickness set to be 10, 12, 14, 16 and 18 mm are simulated. Increasing the
204 thickness of a steel deck layer can also reduce the maximum tensile strain effectively. It is observed
205 that 2 mm thicker steel deck layer can reduce the maximum tensile strain on top of PA layer by 25%
206 is drawn, Figure 13.

Strain XX on mid. top of PA

207

FIGURE 13 Maximum tensile strain on top of PA (steel deck thickness varies)

Effect of the Stiffness of upper and bottom membrane layers

210   Relaxation tests have been used to determine the Zener model parameter to simulate the Visco-Elastic
211   response of the membrane layer. The model parameters are listed Table 1. The parameters at $10\,C^o$
212   are regarded as standard set of parameters for both top and bottom membranes. Simulations that the
213   set of membrane parameters are magnified as 3 and 5 times larger are done for comparison.
214   The stiffness of the two membrane layers plays a quite important role in combining different
215   surfacing material layers together as a whole. Assume that the stiffness of membranes is comparable
216   with PA or GA layers, and those layers are properly bonded together, the multilayer surfacing
217   structure could be regarded as a composite beam. While when the membranes layers are quite soft or
218   the bond condition is too week, all those material layers would behave separately. This phenomena
219   could be testified by the strain distributions at section 1-1 and 2-2, Figure 14.
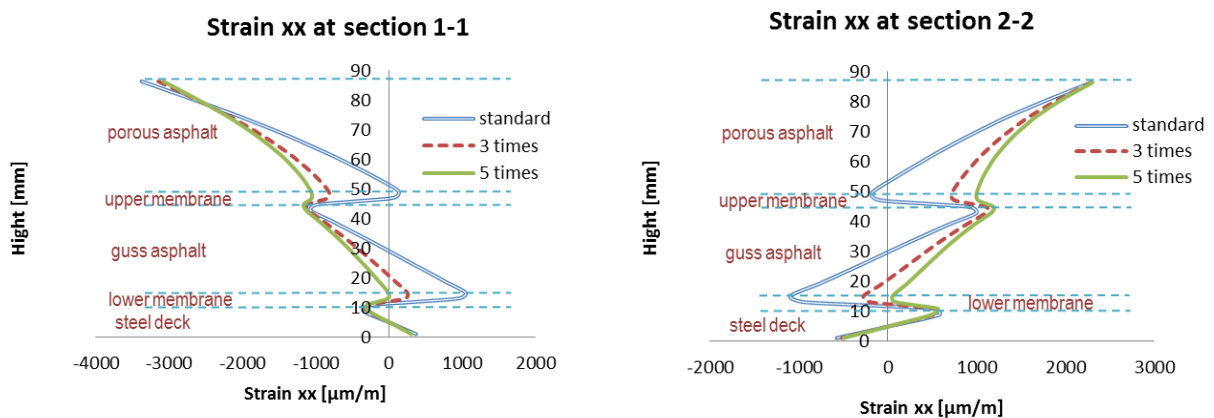

FIGURE 14 Transversal strain at section 1-1 & 2-2 (membrane stiffness varies)

220   Basic on the results shown in Figure 14, the following remarks can be made.
221   •   Stiffer membranes allow better composite behavior of the surfacing structure. The higher
222   stiffness of the membranes (closer to the stiffness of PA or GA) is, the closer mechanical
223   behavior to the linear elastic theory could obtained.
224   •   There are less effects on the tensile strain on the top of PA layer when the stiffness of
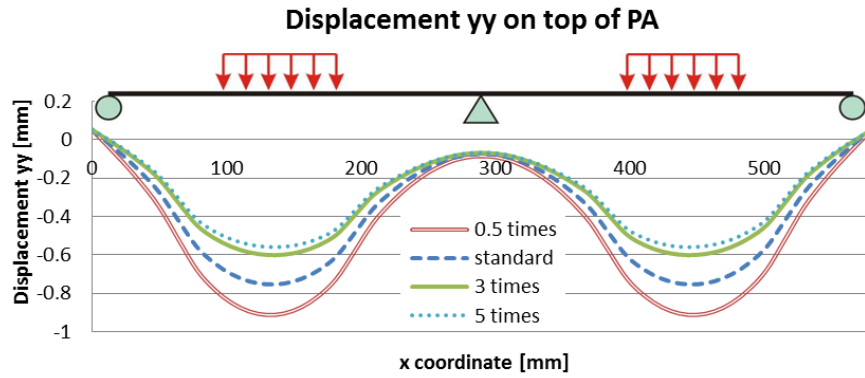225   membranes are increased.
226   Figure 15 shows the deflection curves on top of porous asphalt layer. The sensibility of
227   membrane stiffness to the whole surfacing structure is quite significant at low stiffness values and
228   becomes less sensitive when the stiffness comes to a considerable high level.

229

230   **FIGURE 15 Vertical deformation on top of PA (membrane stiffness varies)**

231   **Effect of environmental temperatures**

232   Basic on the model parameters at 10 and -5 $^{\circ}$C (Table 1), simulations are done and the FEM results
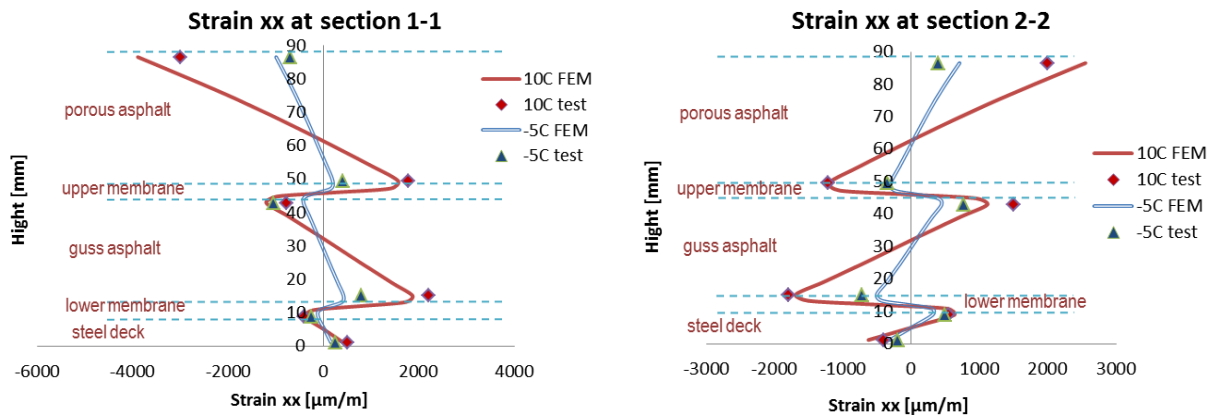233   are compared together with the tests data, see Figure 16.

                        FIGURE 16 Transversal strain at section 1-1& 2-2 (10 $^{\circ}$C and -5 $^{\circ}$C)

234   It can be observed that the FEM results have good agreement with the experimental results.
235   The response of the surfacing structure differs significantly at different temperatures due to the
236   temperature sensitivity of asphaltic materials. The lower the environmental temperature is, the stiffer
237   the surfacing structure will be.

238   **CONCLUSIONS**

239   The main findings from the results presented in this paper are summarized as follows.
240   • The five-point bending test offers a good tool in studying the composite behavior of the
241   multilayer surfacing system on OSDB;
242   • The analytical solution is useful in understanding the numerical results. Furthermore, it
243   provides a guild tool for experiment test design;
244   • A thicker steel plate can significantly reduce the maximum tensile strain as well as the
245   deflection of the structure;
246   • The thickness of PA layer can influence the maximum tensile strain and deflection of the
247   structure. Compared with the influences of PA, the thickness variation of GA is more
248   effective;
249   • Stiffer membranes used in the multilayer surfacing system will result in a lower structure
250   deflection and influence the transversal strain distribution in PA and GA layers , However it
251   has less influence on the maximum tensile strain on the top of PA layer.

252   • A stiffer membrane results in higher strain and stress inside membrane material itself, which
253   may cause its failure. Special attention should be paid to the strength of membrane materials.
254

ACKNOWLEDGMENT

REFERENCE

261 1.   Gurney, T. Fatigue of steel bridge decks. HMSO Publication Centre: London. 1992, pp. 165.
262 2.   Mangus, A.R. and S. Sun. *Orthotropic Bridge Decks. Bridge Engineering Handbook*, ed. W.
263   Chen and L. Duan 1999, Boca Raton: C.R.C. Press.
264 3.   Medani, T.O. *Design principles of surfacings on orthotropic steel bridge decks*. Delft
265   University of Technology, Delft, 2006.
266 4.   Hameau, G., C. Puch, and A.M. Ajour. Revetements de Chaussees Sur Platelages Metalliques
267   -2-Comportement a La Fatigue En Flexion Sous moment Negati, 1981.
268 5.   Scarpas, A. *A Mechanics Based Computational Platform for Pavement Engineering*. TU Delft
269   publication, 2004.
270 6.   Pouget, S., et al. Numerical simulation of the five-point bending test designed to study
271   bituminous wearing courses on orthotropic steel bridge. *Materials and Structures*, 43(3), 2010,
272   pp. 319-330.
273 7.   Houel, A., T.L. N'Guyen, and L. Arnaud. Monitoring and designing of wearing courses for
274   orthotropic steel decks throughout the five-point bending test. *Advanced Testing and
275   Characterisation of Bituminous Materials*, Vols 1 and 2, 2009, pp. 433-442.
276 8.   Freitas, T.d. *Steel plate reinforcement of orthotropic bridge decks, in Structural and Building
277   Engineering*. Civil Engineering and Geosciences, Delft University of Technology,Delft, 2012.
278 9.   Liu, X., and A. Scarpas. *Experimental and Numerical Characterization of Membrane Adhesive
279   Bonding Strength on Orthotropic Steel Deck Bridge*s, *Part 1*. Project report, Delft University
280   of Technology, 2012.
281 10.   Van den Bosch, M.J., Schreurs, P.J.G., and M.G.D. Geers. An improved description of the
282   exponential Xu and Needleman cohesive zone law for mixed-mode decohesion. *Eng. Frac.
283   Mech*. 73, 2006, pp. 1220-1234.
284

285